10-1-2007

Gold nanorods mediate tumor cell death by compromising membrane integrity

Ling Tong
Purdue University - Main Campus, lingt@purdue.edu

Yan Zhao
Purdue University - Main Campus

Terry B. Huff
Purdue University - Main Campus, tbhuff@purdue.edu

Matthew N. Hansen
Purdue University - Main Campus

Alexander Wei
Purdue University - Main Campus, alexwei@purdue.edu

See next page for additional authors

ADVANCED MATERIALS

DOI: 10.1002/adma.200701974

Gold Nanorods Mediate Tumor Cell Death by Compromising Membrane Integrity**

By *Ling Tong*, *Yan Zhao*, *Terry B. Huff*, *Matthew N. Hansen*, *Alexander Wei*,* and *Ji-Xin Cheng**

Light-activated therapies can be used to eradicate diseased cells and tissues in a non-invasive manner. Much attention has been focused on the emerging potential of photothermolysis (also referred to as optical hyperthermia), which involves the conversion of absorbed light into heat via nonradiative mechanisms. Photoactivated effects can be localized and intensified by employing exogenous agents with large absorption cross-sections, confining damage to areas of interest with minimal collateral effects.[1] In particular, targeted photothermolysis may be most effective when mediated by photothermal agents that absorb strongly at near-infrared (NIR) frequencies, to enable deeper penetration into biological tissues.[2]

Among the many materials investigated for NIR photoactivated imaging and therapy, plasmon-resonant gold nanorods (GNRs) and nanoshells appear to be some of the most effective agents to date.[3–7] GNRs can be prepared with lengths on the order of 50 nm,[8–10] a size compatible with long blood residency and permeation into tumors via their leaky vasculatures. GNRs support longitudinal plasmon resonances at NIR frequencies with higher quality factors than those of spherical gold nanoparticles at comparable resonance frequencies[11,12] and are highly efficient at converting light energy into heat, particularly if embedded in media of low thermal conductivity.[13] Recently, GNRs have been shown to be capable of generating two-photon luminescence (TPL) at sufficient intensities for single-particle detection and *in vivo* imaging.[14,15] This latter property permits the real-time imaging of GNRs during their simultaneous application as photothermal agents in biological systems.[16]

While the therapeutic potential of nanoparticle-mediated photothermolysis is widely recognized, many causal relationships between local photothermal effects and cell injury remain to be defined. Heat-induced cell injury has traditionally been viewed as a systemic effect, characterized by phenotypic responses such as membrane blebbing, depolymerization of cytoskeletal filaments, thermal inactivation of membrane proteins and mitochondria, or increased production of heat shock proteins.[17–19] These individual outcomes may be resolved at the subcellular level by using targeted nanoparticle delivery to administer localized photothermal effects.[20–25] For example, nanosecond laser pulses have been used to induce cavitation in cells containing gold nanoparticles, resulting in transient increases in membrane permeability and inactivation of adsorbed proteins.[20,21] These processes are quite distinct from those based on systemic changes in temperature.

In this work we investigate the mechanisms and extent of photothermal injury inflicted by GNRs targeted to cell-surface receptors. Folate-conjugated GNRs were monitored in real time by TPL microscopy, and were observed to be particularly effective at inducing tumor cell necrosis when localized on the cell membrane. The mechanistic insights in this study reveal that the photothermal activity of GNRs and other nanoparticles extends beyond simple hyperthermia, and can be directed for maximum damage to cells using an appropriate targeting mechanism.

GNRs (λ_{max} = 765 nm) were prepared as previously described[8,9] and functionalized with a folic acid conjugate by *in situ* dithiocarbamate formation, a recently developed method for the robust functionalization of gold surfaces (Fig. 1).[16,26] The folate-conjugated nanorods (F-NRs) were targeted toward the plasma membrane of malignant KB cells, a tumor cell line known to overexpress the high-affinity folate receptor.[27] Cells were observed to be densely coated with F-NRs

[*] Prof. A. Wei, Prof. J.-X. Cheng, L. Tong, Dr. Y. Zhao, T. B. Huff, M. N. Hansen
Department of Chemistry, Purdue University
West Lafayette, IN 47907 (USA)
E-mail: alexwei@purdue.edu; jcheng@purdue.edu
Prof. J.-X. Cheng
Weldon School of Biomedical Engineering, Purdue University
West Lafayette, IN 47907 (USA)

[**] This work was supported by the National Institutes of Health (EB-001777), the National Science Foundation (CHE-0243496), and a grant from the Oncological Sciences Center at Purdue University. The authors thank Hongtao Chen for his assistance in SPT analysis, Professor Philip Low for providing folate-Bodipy and KB cells, and Professor Stephen Konieczny for providing NIH-3T3 cells. Supporting Information is available online from Wiley InterScience or from the authors.

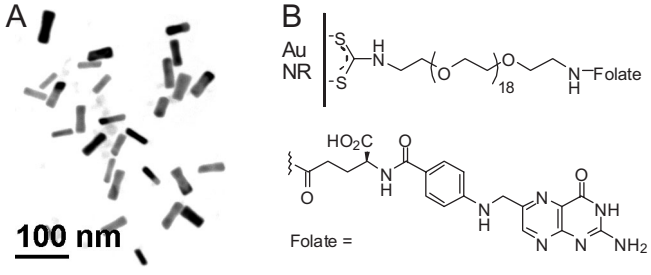

Figure 1. (A) Transmission electron micrograph (JEOL 2000FX, 200 kV) of gold nanorods (λ_{max} = 765 nm), prepared by seeded growth method. (B) Folate–oligoethyleneglycol ligands, conjugated onto gold nanorod surfaces by *in situ* dithiocarbamate formation.

after 6 h incubation using TPL microscopy (Fig. 2A); the membrane-bound F-NRs could be dislodged by washing the cells with a pH 3.3 buffer. F-NRs were also applied to cultured NIH-3T3 cells having low folate receptor expression with little binding observed after 6 h, confirming the targeted nature of nanorod adsorption (Fig. 2C). The receptor-bound F-NRs were very slowly internalized, but observed to be fully translocated to the perinuclear region after 17 h (Fig. 2B). The intracellular translocation of F-NRs by KB cells was further characterized by single particle tracking analysis and exhibited a bidirectional motion towards the nucleus and the plasma membrane, fully consistent with a directed motion model (Fig. S2). The profile for F-NR cell uptake is in stark contrast to that of molecular folate conjugates, which under similar conditions have an uptake rate on the order of minutes.[28]

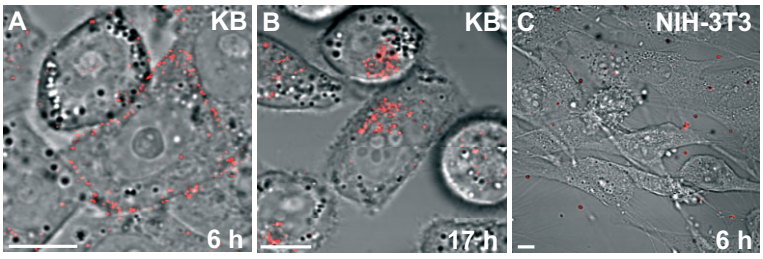

Figure 2. Targeted adsorption and uptake of folate-conjugated GNRs (F-NRs, red) by KB cells overexpressing folate receptors (imaged in transmission mode, grey). (A) A high density of F-NRs was observed on the surface of KB cells after 6 h incubation at 37 °C. (B) F-NRs were internalized into KB cells and delivered to the perinuclear region after 17 h incubation. (C) No binding was observed of F-NRs to NIH-3T3 cells, which express folate receptors at a low level. Scale bar = 10 μm.

KB cells incubated with F-NRs were scanned continuously for 81.4 s (49 scans, 1.66 s per scan) with a tightly focused continuous-wave (cw) laser beam, tuned to the plasmon resonance at 765 nm. Cells with membrane-bound F-NRs (Fig. 3A and B) suffered from photoactivated damage after scanning in cw mode, at powers as low as 6 mW at the sample (mean power density and fluence of 388.8 W cm^{-2} and 24 J cm^{-2}, respectively). Evidence for photoinduced injury includes heavy nuclear staining by ethidium bromide (EB), indicating loss of membrane integrity,[29] accompanied by extensive and irreversible membrane blebbing, a generally accepted sign of cell death.[30]

The threshold for photoinduced damage is strongly affected by the site of F-NR localization,

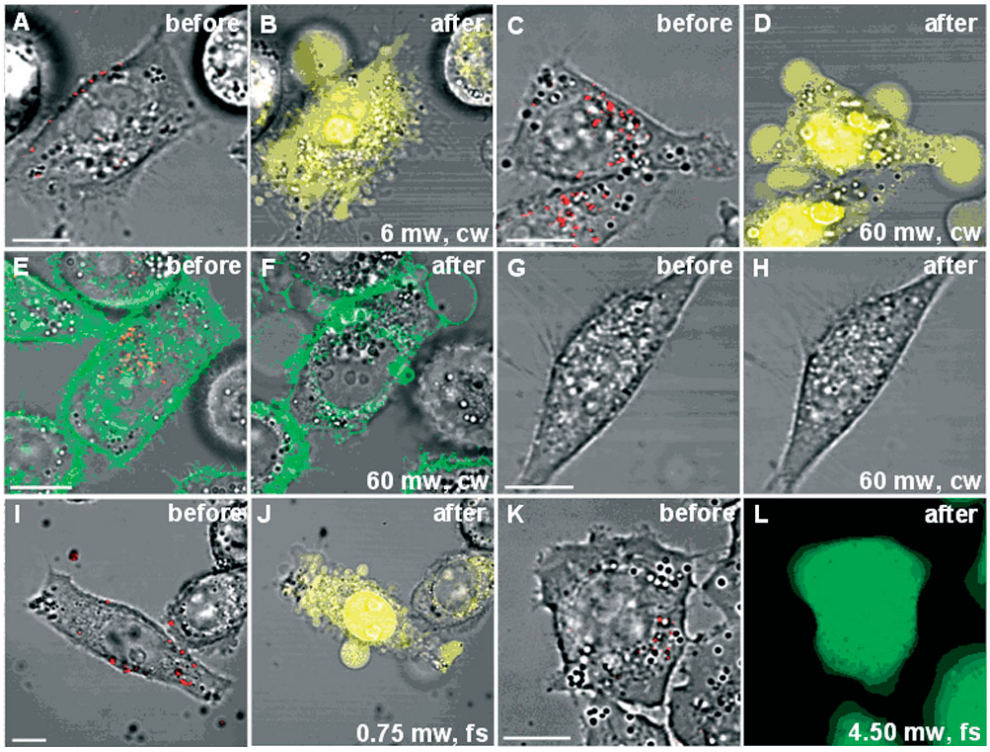

Figure 3. Site-dependent photothermolysis mediated by F-NRs (red). (A,B) Cells with membrane-bound F-NRs exposed to cw NIR laser irradiation experienced membrane perforation and blebbing at 6 mW power. The loss of membrane integrity was indicated by EB staining (yellow). (C,D) Cells with internalized F-NRs required 60 mW to produce a similar level of response. (E,F) F-NRs internalized in KB cells labeled by folate-Bodipy (green) were exposed to laser irradiation at 60 mW, resulting in both membrane blebbing and disappearance (melting) of the F-NRs. (G,H) NIH-3T3 cells were unresponsive to F-NRs, and did not suffer photoinduced damage upon 60 mW laser irradiation. (I,J) Cells with membrane-bound F-NRs exposed to fs-pulsed laser irradiation produced membrane blebbing at 0.75 mW. (K,L) Cells with internalized F-NRs remained viable after fs-pulsed irradiation at 4.50 mW, as indicated by a strong calcein signal (green).

ADVANCED MATERIALS

similar to a recently reported case involving gold nanoclusters.[23] Cells with internalized F-NRs (Fig. 3C and D) required a cw irradiation power of 60 mW to induce a membrane blebbing response, an order of magnitude greater than in the case of membrane-bound F-NRs. The temporal localization of membrane-bound F-NRs noted above suggests an optimum time window for photoactivated therapy, following the delivery of nanorods to cell surfaces but prior to their internalization.

Several factors may contribute toward the greater efficacy of the latter: i) thermal disruption of the membrane provides the most direct opportunity to inflict cell damage; ii) the accumulation of nanorods on the surface focuses photothermal effects into a confined area; and iii) the relatively low thermal conductivity of the cell membrane may contribute toward larger temperature gradients with subsequently more intense hyperthermic effects.[13] It is also worth mentioning that the TPL signals were greatly diminished after cw irradiation at high power, signifying that most of the GNRs had melted and were no longer resonant at NIR frequencies.

To verify that blebbing was due to morphological changes in the membrane, KB cells with internalized F-NRs were treated with folate-Bodipy for 30 min prior to cw irradiation (Fig. 3E). The boundary of the resulting blebs was clearly fluorescent (Fig. 3F), confirming photoinduced deformation of the cell membrane. In control experiments, cells devoid of nanorods were unaffected by either cw or fs-pulsed irradiation at the powers used in our studies (Fig. 3G and H) and cells with internalized F-NRs were healthy after 24 h of dark incubation (Fig. S3). These results indicate that the observed cell injuries are due solely to F-NR-mediated photothermal effects.

Membrane-bound F-NRs were even more effective at inflicting photoinduced injury under femtosecond (fs)-pulsed laser irradiation. Tumor cells with membrane-bound F-NRs exhibited strong EB staining and blebbing (Fig. 3I and J) after scanning at a reduced average power of 0.75 mW, corresponding to a pulse energy of 9.7 pJ (mean power density and fluence of 48.6 $W\,cm^{-2}$ and 3 $J\,cm^{-2}$, respectively). KB cells with membrane-bound F-NRs were monitored in real time while exposed to a fs-pulsed laser beam, and produced clearly visible membrane blebs within 10 s of irradiation (Supporting Fig. S4). In contrast, KB cells with internalized F-NRs remained viable after fs-pulsed irradiation at a higher power of 4.5 mW (Fig. 3K and L), as indicated by a strong intracellular calcein fluorescence. The site-dependent photoinduced damage under fs-pulsed conditions is consistent with the results above using cw irradiation.

The increased efficiency of photothermolysis under fs-pulsed conditions can be attributed to the ultrafast electron dynamics involved in plasmon-mediated heating. The photothermal activity of GNRs is driven primarily by thermalization of the conduction electrons on the fs timescale, followed by electron–phonon relaxation on the picosecond timescale and subsequent thermalization of the phonon lattice.[31] GNRs also have a plasmon-enhanced two-photon absorption cross section[14,32] which further increases the population and energy of photoexcited electrons under fs-pulsed conditions. Electronic thermalization is followed by transient plasmon bleaching, the recovery rate of which is on the order of picoseconds.[31] Such plasmon bleaching has little effect on the absorption efficiency of GNRs exposed to a train of fs pulses with nanosecond intervals for plasmon relaxation; on the other hand, GNRs under cw irradiation are continuously saturated, which reduces their absorption efficiency and overall photothermal energy conversion.

It must be noted that ultrafast laser pulses of sufficiently high energy can be applied directly toward single-cell laser surgery with subcellular precision,[33] as demonstrated recently by the intracellular scission of actin filaments.[34] However, the threshold for optical breakdown in the absence of a photosensitizing agent requires pulse energies in the nanojoule range.[33–35] In the presence of GNRs, the threshold for photoinduced damage is reduced to pulse energies in the picojoule range.

With respect to the mechanisms of F-NR-mediated cell death, several recent studies have shown that the photothermal response of plasmon-resonant nanoparticles is intimately linked with cavitation dynamics.[20–25] The gradient for cavitation-induced heating declines sharply from the epicenter, such that direct thermolysis would be limited to targeted cells near the sites of photothermal transduction.[20,23,24] Cavitation is also responsible for transient bubble formation, which can expand by as much as several microns during their microsecond lifespans.[22,33] These microbubbles have been proposed to cause a temporary rupture in cell membranes,[20,21,25] thereby increasing their permeability to EB and other chemical agents.

In our study, the most dramatic effect of F-NR-mediated photothermolysis was the blebbing of the plasma membrane, which occurred within seconds of laser irradiation (Fig. 3). However, bleb formation could not be the direct product of cavitation, as the rates of growth were several orders of magnitude slower than the timescale for microbubble expansion. Furthermore, blebbing was often induced at sites remote from the F-NRs. This could be observed in real time while monitoring KB cells with membrane-bound F-NRs by bright-field and TPL imaging: Exposure to a fs-pulsed laser with 0.75 mW at the sample resulted in bleb formation and the retraction of filopodia within seconds, both close to and far away from the F-NR binding sites (see Supporting Movie 1).

We hypothesized that the blebbing response was due to the disruption of actin filaments, which form a dense 3D network beneath the cell membrane to provide mechanical support and sustain cell shape. This was tested by using KB cells expressing actin-GFP, followed by incubation with F-NRs for 17 h. Exposing these cells to cw laser irradiation (90 mW) for a 81.4 s scan period resulted in membrane blebbing and retraction of filopodia, accompanied by a nonuniform redistribution of actin-GFP and a 53% decrease in overall fluorescence intensity (Fig. 4A and B). KB cells without F-NRs were also exposed to cw laser irradiation and did not experience

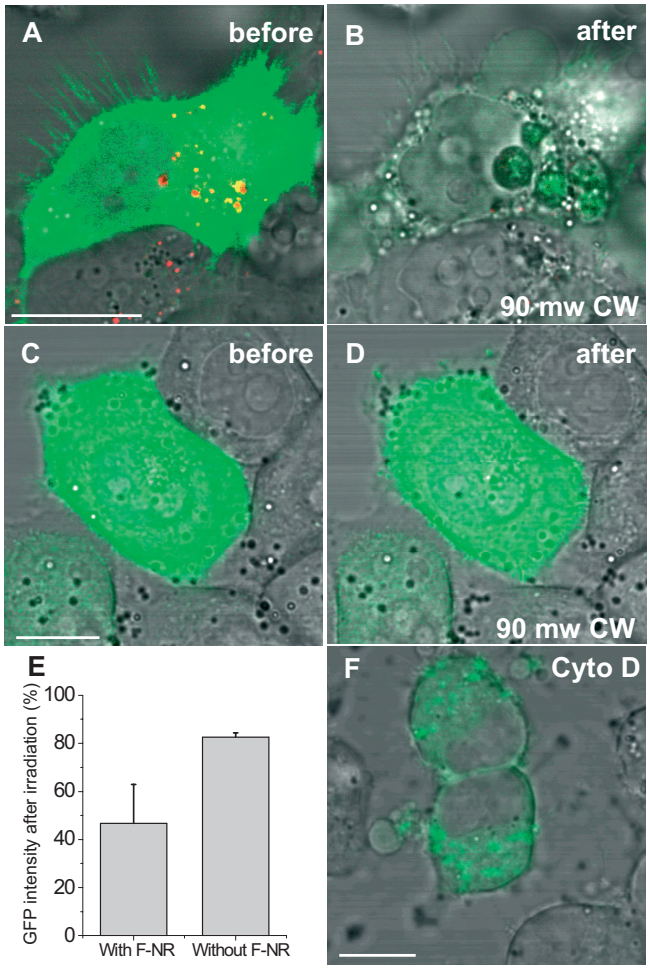

Figure 4. F-NR-mediated disruption of actin filaments in actin-GFP (green) transfected KB cells. (A) KB cell with internalized F-NRs (red) before cw laser irradiation. (B) Membrane blebbing accompanied by redistribution of actin-GFP and loss of fluorescence, after an 81.4 s exposure to cw irradiation at 90 mW. (C,D) KB cells without F-NRs, which did not experience membrane blebbing after exposure to cw irradiation at 90 mW. (E) Histogram showing the decrease in actin-GFP fluorescence intensity in cells with and without F-NR labeling (N=5) after cw irradiation. The minor reduction of fluorescence in cells without F-NR labeling is attributed to photobleaching. (F) Blebbing, redistribution of actin-GFP, and loss of fluorescence in KB cells after 2 h treatment with cytochalasin D (5 μg mL^{-1}). Scale bar = 10 μm.

membrane blebbing (Fig. 4C and D), although actin-GFP fluorescence decreased by 17.5% due to photobleaching (Fig. 4E). In a second control experiment, KB cells without F-NRs were treated for 2 h with cytochalasin D, a potent inhibitor of actin polymerization. These cells exhibited membrane blebs similar to those induced by F-NRs, again accompanied by an attenuated and nonuniform distribution of actin-GFP (Fig. 4F). The blebbing response to F-NR-mediated photothermolysis can thus be correlated with the degradation of the intracellular actin network.

We further considered whether actin filament disruption could be due to an influx of Ca^{2+}, mediated by cavitation-induced perforation of the cell membrane. Elevated concentrations of intracellular Ca^{2+} can result in the detachment of actin filaments from the plasma membrane via the activation of proteases such as calpain.[36] Toxins such as $HgCl_2$[37] and maitotoxin[38] have also been shown to induce membrane blebs by increasing Ca^{2+} influx. To examine the role of Ca^{2+} in photoinduced cell injury, we irradiated KB cells with membrane-bound F-NRs in Ca^{2+}-free phosphate-buffered saline (PBS) as well as in PBS containing 0.9 mM Ca^{2+} (100 mg L^{-1} $CaCl_2$), using fs-pulsed laser irradiation at 3 mW for a 61.5 s scan period. For KB cells irradiated in the presence of Ca^{2+}, membrane blebbing was observed immediately after laser irradiation and accompanied by EB staining, indicating increased membrane permeability (Fig. 5A–C). A strong Oregon Green signal was also produced in the cytoplasm (Fig. 5C), confirming an increased level of intracellular Ca^{2+} in response to the photoinduced injury. For KB cells in Ca^{2+}-free PBS, strong EB staining was also observed, but no blebs were produced (Fig. 5D–F). In a separate experiment, F-NR labeled cells were first irradiated in Ca^{2+}-free PBS and confirmed to have normal morphologies (Fig. 5G, H), whereupon treatment with Ca^{2+} resulted in immediate bleb formation (Fig. 5I). Collectively, these results demonstrate that membrane blebbing is a consequence of Ca^{2+} influx into cells that occurs during F-NR-mediated photothermolysis. It should be noted that in addition to membrane blebbing, Ca^{2+} influx is responsible for inducing a variety of secondary damages, many of which lead to cell death.[36]

In summary, folate-conjugated gold nanorods can be targeted to tumor cells in a site-dependent manner for maximum delivery of photoinduced injury using NIR irradiation. The photothermolysis of KB cells is most effective when F-NRs are adsorbed to the cell surface prior to uptake, with a tenfold difference in damage threshold relative to cells with internalized F-NRs. The nanorods' efficacy is further intensified under fs-pulsed excitation conditions, due to the increased efficiency of NIR absorption and photothermal energy conversion. Cell death is attributed to the disruption of the plasma membrane as a consequence of F-NR-mediated cavitation. Membrane perforation led to an influx of extracellular Ca^{2+} followed by degradation of the actin network, producing a dramatic blebbing response. Nanorods targeted to other cell-surface biomarkers can be expected to produce similar membrane-compromising effects. These results are a significant departure from earlier assumptions regarding nanoparticle-mediated hyperthermia, and provide a foundation for developing targeted photothermolysis for cancer therapy.

Experimental

Preparation and Characterization of F-NRs. Gold nanorods with longitudinal plasmon resonances centered at 765 nm were prepared in high yields in the presence of cetyltrimethylammonium bromide (CTAB) and silver nitrate using seeded growth conditions,[8] then treated with sodium sulfide 30 min after injection of the seed solution to arrest further growth and changes in their optical resonances.[9] The

ADVANCED MATERIALS

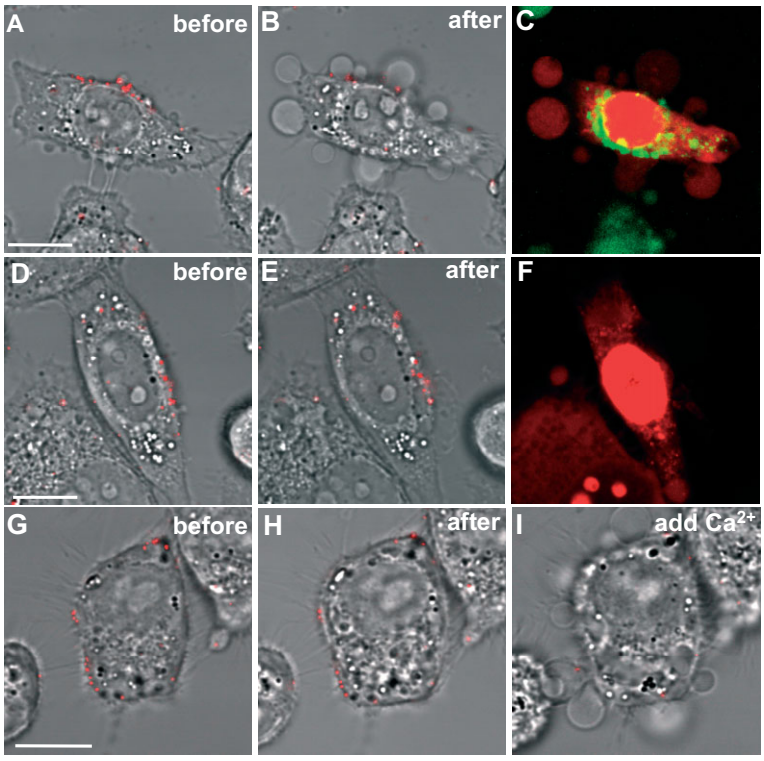

Figure 5. Membrane blebbing is induced by Ca^{2+} influx during F-NR-mediated photothermolysis. (A,B) Cells with membrane-bound F-NRs (red) in PBS containing 0.9 mM Ca^{2+} (100 mg/L $CaCl_2$) exhibited blebbing after exposure to fs-pulsed laser irradiation at 3 mW for 61.5 s. (C) Incubation with 2.5 μM EB (red) and 2 μM Oregon Green 488 for 20 min indicated a compromise in membrane integrity and an elevation in intracellular Ca^{2+}, respectively. (D, E) Cells with membrane-bound F-NRs in Ca^{2+}-free PBS were visibly unchanged by fs-pulsed laser irradiation at 3 mW. (F) Incubation with 2.5 μM EB for 15 min revealed perforation of the cell membrane. (G–I) F-NR labeled KB cells in Ca^{2+}-free PBS were unaffected by fs-pulsed irradiation as described above, but immediately produced blebs upon exposure to 0.9 mM Ca^{2+}. For all experiments, cells were incubated with F-NRs for 6 h, then washed 5 times in PBS with 0.9 mM Ca^{2+} (A–C) or without Ca^{2+} (D–H). Amounts of dyes and reagents are described as final concentrations in the cell culture medium. Scale bar = 10 μm.

nanorods were centrifuged and redispersed in deionized water two times (24000 *g*, 5 min per cycle) to remove CTAB and residual inorganic species, then diluted to an optical density (O.D.) of 1.0–1.2. Particle size analysis by transmission electron microscopy indicated a mean length and aspect ratio of 46.5 nm and 3.7, respectively.

Amine-terminated oligoethyleneglycol chains were tethered onto nanorods by *in situ* dithiocarbamate formation, a recently developed method for the robust functionalization of gold surfaces.[16,26] An aqueous suspension of CTAB-coated nanorods (3 mL, O.D. 1) was treated with a mixed-bed ion-exchange resin (Amberlite MB-3, Sigma) for 10 h at room temperature, then decanted and treated while stirring with a 10-mM solution of *O,O′*-bis(2-aminoethyl)octadecaethylene glycol (Fluka) adjusted to pH 9.5 (1 mL), followed by a saturated solution (28 mM) of freshly distilled CS_2 (0.1 mL). The mixture was stirred for 12 h, then subjected to membrane dialysis for 2 h (MWCO 6000-8000). The amine-coated nanorods were then treated with a 10 μM DMSO solution of *N*-hydroxysuccinimidyl folate (0.2 mL) prepared according to literature procedure,[27] followed by additional dialysis for a complete removal of CTAB molecules from the nanorod solution. The latter step is necessary to prevent nonspecific nanorod uptake.[39] This procedure yielded a stable dispersion of F-NRs with an absorption maximum at 765 nm and a final optical density close to 1. The absorption spectra of the nanorods used in this study were not significantly affected by surface functionalization. The nanorod concentration is on the order of 0.2 nM, estimated from recent experimental measurements of extinction coefficients.[40] The mean hydrodynamic diameter of the F-NRs was determined to be 81.5 nm by TPL correlation spectroscopy (Supporting Fig. S1).

Cell Culture. KB cells and NIH/3T3 cells were cultured at 37 °C in a humidified atmosphere containing 5% CO_2 and grown continuously in folate-deficient RPMI 1640 medium (Invitrogen) containing 10% fetal bovine serum (Sigma) and 1% penicillin-streptomycin (Invitrogen). In a typical experiment, a 1-mL suspension of KB cells (10^5 cells mL^{-1}) was plated onto a coverslip-bottomed Petri dish (MatTek), grown for 2-3 days, then treated with an aliquot of F-NRs (100 μL) and maintained at 37 °C with periodic monitoring.

Two-photon Luminescence Imaging. A femtosecond (fs) Ti:Sapphire laser (Mira 900, Coherent Inc.) with a duration of 200 fs and a repetition rate of 77 MHz was used for TPL imaging of nanorods. The laser beam was directed into a scanning confocal microscope (FV300/IX70, Olympus America Inc.) equipped with a 60X water-immersion objective (NA = 1.2). The excitation power used was 0.75 mW at the sample, unless otherwise noted. Consecutive real-time images (movies) were recorded at a speed of 0.6 frames per second, using the TPL signal to visualize nanorods and the transmission signal to visualize KB cells.

F-NR Mediated Photothermolysis. KB cells incubated with F-NRs were rinsed with fresh RPMI 1640 medium prior to scanning with the Ti:sapphire laser, which could be readily switched between fs-pulsed and cw mode. Cells were irradiated at 765 nm using either mode under constant average power, ranging from 0.75 to 60 mW at the sample. The mean power density was calculated by dividing the average laser power with the scanning area. The exposure time for individual nanorods was calculated as follows. Typically, a 39.3 × 39.3 μm^2 area was scanned at a rate of 1.66 s per scan. Each scan was compiled with 512 × 512 pixels (pixel area = 77 × 77 nm^2; exposure time = 6.3 μs per pixel per scan). The focal spot area was calculated as $\pi d^2/4$, where $d = 0.61\ \lambda/NA$ is the full width at half maximum of the beam waist. In one scan, the exposure time for a nanorod was calculated as (focal spot area / pixel area) × 6.3 μs = 0.126 ms. The total illumination time was calculated as the product of 0.126 ms times the number of scans.

Cell death was determined using 2.5 μM ethidium bromide (EB), a nuclear stain used to test membrane integrity;[29] cell viability was determined using 2.5 μM calcein AM.[5,20] For enhanced observation of the plasma membrane morphology, KB cells were treated with 100 nM folate–boron dipyrromethene difluoride conjugate (folate–Bodipy) which binds to the folate receptor on the cell surface. For monitoring the integrity of actin filaments, KB cells were transfected with plasmids encoded for β-actin conjugated to green fluorescent protein (actin–GFP) using a transfection agent (FuGENE 6), three days prior to photothermal treatment. For pharmacological disruption of actin filaments, KB cells were incubated with 5 μg mL^{-1} cytochalasin D for 2 h prior to observation. To study the role of Ca^{2+} in membrane blebbing, F-NR labeled KB cells were washed with PBS without Ca^{2+} or with 0.9 mM Ca^{2+} (100 mg L^{-1} $CaCl_2$) for 5 times then exposed to laser irradiation. In addition to testing membrane integrity with 2.5 μM EB, irradiated cells were treated with 2 μM Oregon Green 488 (BAPTA-2 AM, Invitrogen) as an indicator of intracellular Ca^{2+}. Fluorescence imaging was carried out on a confocal microscope (FV300/I70, Olympus). A 488-nm Ar^+ laser was used for excitation with 37.5 μW at the sample. The amount of all dyes and reagents

reported here are provided as final concentrations, following dilution in the cell culture medium.

Received: August 3, 2007

[1] R. R. Anderson, J. A. Parrish, *Science* **1983**, *220*, 524.
[2] F. Helmchen, W. Denk, *Nat. Methods* **2005**, *2*, 932.
[3] L. R. Hirsch, R. J. Stafford, J. A. Bankson, S. R. Sershen, B. Rivera, R. E. Price, J. D. Hazle, N. J. Halas, J. L. West, *Proc. Natl. Acad. Sci. USA* **2003**, *100*, 13549.
[4] D. P. O'Neal, L. R. Hirsch, N. J. Halas, J. D. Payne, J. L. West, *Cancer Lett.* **2004**, *209*, 171.
[5] C. Loo, A. Lowery, J. West, N. Halas, R. Drezek, *Nano Lett.* **2005**, *5*, 709.
[6] X. Huang, I. H. El-Sayed, W. Qian, M. A. El-Sayed, *J. Am. Chem. Soc.* **2006**, *128*, 2115.
[7] H. Takahashi, T. Niidome, A. Nariai, Y. Niidome, S. Yamada, *Chem. Lett.* **2006**, *35*, 500.
[8] T. K. Sau, C. J. Murphy, *Langmuir* **2004**, *20*, 6414.
[9] D. A. Zweifel, A. Wei, *Chem. Mater.* **2005**, *17*, 4256.
[10] J. Pérez-Juste, L. M. Liz-Márzan, S. Carnie, D. Y. C. Chan, P. Mulvaney, *Adv. Funct. Mater.* **2004**, *14*, 571.
[11] C. Sönnichsen, T. Franzl, T. Wilk, G. von Plessen, J. Feldmann, O. Wilson, P. Mulvaney, *Phys. Rev. Lett.* **2002**, *88*, 077402.
[12] P. K. Jain, K. S. Lee, I. H. El-Sayed, M. A. El-Sayed, *J. Phys. Chem. B* **2006**, *110*, 7238.
[13] C.-H. Chou, C.-D. Chen, C. R. C. Wang, *J. Phys. Chem. B* **2005**, *109*, 11135.
[14] H. Wang, T. B. Huff, D. A. Zweifel, W. He, P. S. Low, A. Wei, J.-X. Cheng, *Proc. Natl. Acad. Sci. USA* **2005**, *102*, 15752.
[15] K. Imura, T. Nagahara, H. Okamoto, *J. Phys. Chem. B* **2005**, *109*, 13214.
[16] T. B. Huff, L. Tong, Y. Zhao, M. N. Hansen, J.-X. Cheng, A. Wei, *Nanomedicine* **2007**, *2*, 125.
[17] K. Bowler, in *Symp. Soc. Exp. Biol., Vol. 41* (Eds.: K. Bowler, B. J. Fuller), Society for Experimental Biology, Cambridge, **1987**, pp. 157.
[18] W. T. Coakley, in *Symp. Soc. Exp. Biol., Vol. 41* (Eds.: K. Bowler, B. J. Fuller), Society for Experimental Biology, Cambridge, **1987**, pp. 187.
[19] P. Wust, B. Hildebrandt, G. Sreenivasa, B. Rau, J. Gellerman, H. Riess, R. Felix, P. M. Schlag, *Lancet Oncol.* **2002**, *3*, 487.
[20] C. M. Pitsillides, E. K. Joe, X. Wei, R. R. Anderson, C. P. Lin, *Biophys. J.* **2003**, *84*, 4023.
[21] C. P. Yao, R. Rahmanzadeh, E. Endl, Z. X. Zhang, J. Gerdes, G. Hüttmann, *J. Biomed. Opt.* **2005**, *10*, 064012.
[22] V. Kotaidis, A. Plech, *Appl. Phys. Lett.* **2005**, *87*, 213102.
[23] V. P. Zharov, E. N. Galitovskaya, C. Johnson, T. Kelly, *Lasers Surg. Med.* **2005**, *37*, 219.
[24] V. P. Zharov, R. R. Letfullin, E. N. Galitovskaya, *J. Phys. D.* **2005**, *38*, 2571.
[25] D. O. Lapotko, E. Lukianova, A. A. Oraevsky, *Lasers Surg. Med.* **2006**, *38*, 631.
[26] Y. Zhao, W. Pérez-Segarra, Q. Shi, A. Wei, *J. Am. Chem. Soc.* **2005**, *127*, 7328.
[27] R. J. Lee, P. S. Low, *J. Biol. Chem.* **1994**, *269*, 3198.
[28] C. M. Paulos, M. J. Turk, G. J. Breur, P. S. Low, *Adv. Drug Deliv. Rev.* **2004**, *56*, 1205.
[29] C. P. Lin, N. W. Kelly, S. A. B. Sibayan, M. A. Latina, R. R. Anderson, *IEEE J. Sel. Top. Quant.* **1999**, *5*, 963.
[30] A. H. Wyllie, J. F. R. Kerr, A. R. Currie, *Int. Rev. Cytol.* **1980**, *68*, 251.
[31] S. Link, M. A. El-Sayed, *Int. Rev. Phys. Chem.* **2000**, *19*, 409.
[32] A. Bouhelier, R. Bachelot, G. Lerondel, S. Kostcheev, P. Royer, G. P. Wiederrecht, *Phys. Rev. Lett.* **2005**, *95*, 267405.
[33] A. Vogel, J. Noack, G. Hüttmann, G. Paltauf, *Appl. Phys. B* **2005**, *81*, 1015.
[34] N. Shen, D. Datta, C. B. Schaffer, P. LeDuc, D. E. Ingber, E. Mazur, *Mech. Chem. Biosystems* **2005**, *2*, 17.
[35] K. König, O. Krauss, I. Riemann, *Opt. Express* **2002**, *10*, 171.
[36] B. F. Trump, I. K. Berezesky, *FASEB J.* **1995**, *9*, 219.
[37] K. A. Elliget, P. C. Phelps, B. F. Trump, *Cell Biol. Toxicol.* **1991**, *7*, 263.
[38] M. Estacion, W. P. Schilling, *BMC Physiology* **2001**, *1*, 2.
[39] T. B. Huff, M. N. Hansen, Y. Zhao, J.-X. Cheng, A. Wei, *Langmuir* **2007**, *23*, 1596.
[40] C. J. Orendorff, C. J. Murphy, *J. Phys. Chem. B* **2006**, *110*, 3990.